approach.[27] Since the reaction involves the formation of two new SiH bonds and the breaking of an H-H bond, the proper MCSCF description requires the inclusion of all configurations generated from the distribution of four electrons among four active orbitals. In the separated reactants, the four active orbitals correspond to the lone pair and empty p orbitals on SiH_2 and the bonding and antibonding orbitals on H_2. Relative to the SCF transition state,[9] this 20-configuration MCSCF with a 6-31G* basis set (MC-(4,4)/6-31G*) results in a small lengthening in the two forming SiH bonds (0.06 and 0.01 Å for the longer and shorter bonds, respectively) and virtually no change in the H-H distance. Grev and Schaeffer[10] (GS) have performed a two-configuration transition-state optimization for this system and obtained a similar structure. The GS H-H distance is about 0.04 shorter, probably a reflection of the incorporation of p functions into the basis set. The MP3//MC(4,4)/6-31G* barrier is found to be 5.2 kcal/mol.

At the MCSCF(4,4)/6-31G* level of computation, the calculated barrier is 16.2 kcal/mol. Addition of second-order configuration interaction (SOCI = all single and double excitations from the 20 MCSCF configurations) incorporates more than 25 000 configurations and reduces the calculated barrier to 8.4 kcal/mol. Note that this is very similar to the MP3/6-31G* result quoted above. Grev and Schaeffer have performed the analogous CI with their two-configuration wave function (~7000 configurations) and found a rather smaller barrier (4.8 kcal/mol). Again, the difference is very likely to be found in their incorporation of p functions on the hydrogens.

Since the MP3/6-31G** barrier for $SiH_2 + H_2$ appears to be fairly insensitive to geometry, a preliminary probe of the effect of hydrogen-polarization functions on the $SiH_2 + CH_4$ reaction was carried out using the geometries quoted in Figure 1. This results in a barrier of 26.8 kcal/mol. As expected, the importance of hydrogen p functions is smaller than for $SiH_2 + H_2$ and still leaves the calculated barrier well above the experimental value. The effect of using multiconfiguration wave functions on this result will be probed in a later paper.

Acknowledgment. This work was supported by the donors of the Petroleum Research Fund, administered by the American Chemical Society. The computer time made available by the North Dakota State University Computer Center is gratefully acknowledged, as are several stimulating discussions with Dr. Michael Schmidt.

Registry No. :CH_2, 2465-56-7; :SiH_2, 13825-90-6; CH_4, 74-82-8; SiH_4, 7803-62-5; H_2, 1333-74-0.

(27) Ruedenberg K.; Schmidt, M. W.; Gilbert, M. M.; Elbert, S. T. *Chem. Phys.* **1982**, *71*, 48.

Thermodynamic and Structural Aspects on Liquid and Solid Benzene. Monte Carlo Study

Per Linse

Contribution from Physical Chemistry 1, Chemical Center, S-220 07 LUND, Sweden.
Received December 12, 1983

Abstract: Liquid and solid benzene have been examined by Monte Carlo simulations using pairwise additive potentials obtained from ab initio quantum chemical calculations. Various experimental data are satisfactorily reproduced by this potential, which generally is an improvement of empirical ones. In the liquid, in comparison with the solid phase, there is almost no angular orientation correlation between pairs of molecules except at very short distances, where the non-spherical exchange repulsion favors the stacked configuration. However, the repulsive quadrupole–quadrupole interaction strongly reduces the probability of the stacked configuration at such short separations. In solid benzene at 258 K, the effective rotational energy barrier is smaller for rotation around the C_6 axis than for rotation around a C_2 axis. The relatively large freedom of rotation around the C_6 axis smooths the otherwise oscillated structure of the atom–atom distribution functions.

I. Introduction

Computer simulations may provide data on structural and dynamic properties of liquids. Liquid benzene has been the subject of several investigations[1-3] by simulation techniques using empirical pair potentials based on site–site interactions. Evans and Watts have investigated several benzene–benzene potentials[4,5] and have used a six-site Lennard–Jones potential to calculate static properties using the Monte Carlo (MC) technique.[1] Steinhauser[2] has reported both structural and dynamic results from molecular dynamics (MD) calculations based on the same potential as in the MC work of Evans and Watts. Claessens et al.[3] showed that an additional point quadrupole, fixed to its experimental value, at the center of the benzene molecule might improve the empirical potential by reducing the probability of the stacked configuration.

This work presents a MC study of liquid and solid benzene based on an ab initio quantum mechanical pair potential.[6] Dynamic aspects on benzene will be deferred to a second paper.

II. Benzene Pair Potentials

The benzene potential used in the present simulations has been described by Karlström et al.[6] It was obtained from ab initio quantum chemical calculations using the Hartree–Fock self-consistent-field (HF-SCF) approximation, and the dispersion energy was obtained by a perturbation procedure. The resulting intermolecular energy function is a linear combination of atom–atom terms of the form

$$E = \sum_i \left[A_i \frac{1}{r_i} + B_i \frac{1}{r_i^4} + C_i \frac{1}{r_i^6} + D_i \frac{1}{r_i^9} + E_i \frac{1}{r_i^{12}} \right] \quad (1)$$

where i sums over the interatomic distances C–C, C–H, and H–H. Table I gives the benzene geometry used and the coefficients for the best fit.

The same quantum chemical data have been used to obtain the best Lennard–Jones (LJ) parameters for four potentials with the same fitting procedure was earlier.[6] Table II shows the potentials, their mean-square deviation, and best LJ parameters with their standard deviations. An analysis of the potentials for different configurations shows that potential 1 is incapable of simultaneously

(1) Evans, D. J.; Watts, R. O. *Mol. Phys.* **1976**, *32*, 93.
(2) Steinhauser, O. *Chem. Phys.* **1982**, *73*, 155.
(3) Claessens, M.; Ferrario, M.; Ryckaert, J.-P. *Mol. Phys.* **1983**, *50*, 217.
(4) Evans, D. J.; Watts, R. O. *Mol. Phys.* **1975**, *29*, 777.
(5) Evans, D. J.; Watts, R. O. *Mol. Phys.* **1976**, *31*, 83.
(6) Karlström, G.; Linse, P.; Wallqvist, A.; Jönsson, B. *J. Am. Chem. Soc.* **1983**, *105*, 3777.

0002-7863/84/1506-5425$01.50/0

Table I. Coefficients of the Fitted Benzene Pair Potential according to Eq 1[a]

atom pair, i	A_i	B_i	C_i	D_i	E_i
C–C	3.0711×10^1	-1.2335×10^2	-1.3623×10^3	6.7001×10^4	8.1342×10^5
C–H	-3.0711×10^1	1.1675×10^2	-1.1997×10^3	6.8714×10^3	1.1582×10^5
H–H	3.0711×10^1	-1.1014×10^2	4.8027×10^2	-2.4698×10^3	1.3059×10^4

[a] Units are in kJ/mol and Å. The benzene molecule was kept rigid with $r_{CC} = 1.395$ Å and $r_{CH} = 1.084$ Å. The mean-square deviation of the fit was 1.0 kJ/mol.

Table II. The Four Potentials of LJ Type[a] and Those Given by Ref 1–3

no.	atom–atom pair	interaction	mean-square deviation, kJ/mol	σ, Å	ϵ/k, K
1	C–C	LJ	3.0	3.3 ± 0.2	40 ± 16
2	C–C	LJ + quadrupole[b]	2.0	3.3 ± 0.1	57 ± 11
3	C–C				
	C–H	LJ	1.3	[c]	[c]
	H–H				
4	C–C			3.3 ± 0.1	43 ± 10
	C–H	LJ + quadrupole[b]	1.1	2.9 ± 0.2	13 ± 12
	H–H			1.9 ± 0.4	110 ± 190
ref 1 and 2	[d]	LJ		3.50	77.0
ref 3	C–C[e]	LJ		3.72	55.3
ref 3	C–C[e]	LJ + quadrupole[f]		3.745	48.0

[a] Same benzene geometry as in Table I. The accuracy of the LJ parameters is given by their standard deviation. [b] $Q = -30 \times 10^{-40}$ Cm^2. [c] No LJ parameters were obtained, since the fitted coefficients gave a repulsive C–C and H–H interaction at all atom–atom distances. However, the molecular interaction is well-behaved due to compensation by C–H interactions. [d] $r_{site-site} = 1.756$ Å. [e] $r_{CC} = 1.410$ Å. [f] Point quadrupole, $Q = -29 \times 10^{-40}$ Cm^2.

describing (i) the repulsive stacked configuration, (ii) the global minimum,[6] and (iii) the correct molecular extension in the plane. An addition of a quadrupole, $Q = -30 \times 10^{-40}$ Cm^2, improves the potentials substantially, but still the benzene molecule is too small in its plane. Potential 3 gives a satisfactory fit except for the stacked configuration, and potential 4 is almost as good as the potential function described by eq 1. Thus, a six-site LJ model is less satisfactory which has also been pointed out previously,[2,3] and both an inclusion of a quadrupole moment and an explicit treatment of the hydrogens do improve the potential.

III. Details of Calculations

General principles of the Monte Carlo method have been reviewed by several authors[7-9] and will not be repeated here. The algorithm of Metropolis et al.[10] was used in the canonical ensemble (N, T, V). All simulations were performed with $N = 108$ benzene molecules in a box with periodic boundary conditions and with a minimum image convention.[9] At intermolecular distances exceeding 10 Å an isotropic potential, obtained from the anisotropic potential (see next paragraph), was used. Both the isotropic potential and the potential according to eq 1 were stored in energy tables. Table III gives the temperature, density, and box lengths for the four simulations performed. All simulations were equilibrated from a *Pbca*[12] orthorhombic lattice with four molecules per unit cell for at least 0.54 million configurations, and the analysis was performed during the following 1.08 million ones. The translational and rotational displacement steps were 0.5 Å and 10.0° except at 120 K where 0.2 Å and 4.0° were used giving an acceptance rate of 40% to 60%.

The introduction of an isotropic potential was done in order to decrease the large number of site–site interaction pairs, which is the bottleneck in the simulation of multisite models. The isotropic potential was also constructed by using the functional form according to eq 1. The sum over i was dropped and $A = 36A_{CC} + 72A_{CH} + 36A_{HH}$ + etc., where A_{CC}, A_{CH}, A_{HH}, etc., were taken from the ansiotropic potential. Since benzene is neutral and there is a linear dependence[6] among B_i, $A = B = 0$, and the $1/r^6$ term becomes the dominating long-range term. This procedure introduces a small positive energy shift in the order of the accuracy of the MC algorithm. The orientational dependence of the potential at large separations arises from the quadrupole–qaudrupole interactions. Since it is much smaller than kT at 10 Å, the effective r dependence becomes $1/r^{10}$, and secondary orientational effects due to the use of the isotropic potential are thus believed to be entirely negligible.

Table III. Data for the Four Simulations

temp, K	exptl state	density, g/cm^3	box lengths, Å		
120	solid	1.098[a]	22.20	28.20	20.37[a]
258	solid	1.031[a]	22.35	28.89	21.03[a]
308	liquid	0.864[b]	23.67	30.69	22.32[c]
348	liquid	0.819[b]	24.09	31.23	22.71[c]

[a] Obtained by interpolation from experimental data, ref 5, Table I. [b] Experimental density from ref 11. [c] Ratio of box lengths according to experimental data at 270 K, ref 12.

IV. Results and Discussion

A. Energy and Heat Capacity. We will compare the calculated configuration energies (E_{conf}^{calcd}) and the configurational contribution to the heat capacity at constant volume ($C_{v,conf}^{calcd}$) with the experimentally determined enthalpy of evaporation (ΔH_{vap}^{exptl}), the total enthalpy (H^{exptl}), and the heat capacity at constant pressure (C_p^{exptl}).

Ignoring excited electronic states, the total energy may be written

$$E = E_t + E_r + E_v + E_{conf} \quad (2)$$

where E_t denotes translational energy, E_r rotational energy, E_v vibrational energy, and E_{conf} configurational energy. The enthalpy may be expressed by

$$H_{(g)} = E_{(g)} + RT \quad (3)$$

$$H_{(l,s)} = E_{(l,s)} \quad (4)$$

assuming ideal benzene vapor and $PV \ll H$ for the condensed phases. Since $\Delta H_{vap} = H_{(g)} - H_{(l,s)}$ we get

$$\Delta H_{vap} = E_{(g)} - E_{(l,s)} + RT \quad (5)$$

We assume that the hindered translational motions and the librations in the solid can be described classically and that the internal vibrations are independent on the phase giving

$$\Delta H_{vap(l,s\to g)} = E_{conf(l,s)} + RT \quad (6)$$

(7) Wood, W. W. In "Physics of Simple Liquids"; Temperley, H. N. V., Rowlinson, J. S., Rushbrooke, G. S., Eds.; North-Holland: Amsterdam, 1968; Chapter 5.
(8) Wood, W. W. In "Fundamental Problems in Statistical Mechanics III"; Cohen, E. G. D., Ed.; North-Holland: Amsterdam, 1975.
(9) Valleau, J. P.; Wittington, S. G.; Valleau, J. P.; Torrie, G. M. In "Modern Theoretical Chemistry"; Berne, B. J., Ed.; Plenum Press: New York, 1977; Vol. 5.
(10) Metropolis, N.; Rosenbluth, A. W.; Rosenbluth, M. N.; Teller, A. H.; Teller, E. *J. Chem. Phys.* **1953**, *21*, 1087.
(11) "Physico-Chemical Constants of Pure Organic Compounds"; Timmermann, J., Ed.; Elsevier: Amsterdam, 1965.
(12) Cox, E. G.; Cruickshank, D. W. J.; Smith, J. A. S. *Proc. R. Soc. London, Ser. A* **1958**, *241*, 1.

Table IV. Thermodynamic Results[a]

T	E_{conf}^{calcd}	E_{cor}^{calcd}[b]	E_{conf}^{calcd}	$C_{v,conf}^{calcd}$
120	−51.3 ± 0.4	−0.9	−52.2	19 ± 2
258	−44.3 ± 0.4	−0.8	−45.1	16 ± 1
308	−33.0 ± 0.3	−0.6	−33.6	15 ± 1
348	−30.1 ± 0.3	−0.5	−30.6	16 ± 2

T	ΔH_{vap}^{calcd} (eq 6)	ΔH_{vap}^{exptl}[c]	$\Delta H_{vap}^{calcd} - \Delta H_{vap}^{exptl}$
120	53.3		
258	47.2	45.7	1.5
308	36.2	33.6	2.6
348	33.5	32.1	1.4

T	E_v	H^{calcd} (eq 7)	$H_T^{calcd} - H_{120}^{calcd}$	$H_T^{exptl} - H_{120}^{exptl}$[d]	$H_T^{calcd} - H_T^{exptl}$
120	0.1	−49.1	0	0	
258	2.6	−36.1	13.0	11.2	1.8
308	4.8	−21.1	28.0	27.6	0.4
348	7.1	−14.8	34.3	33.3	1.0

[a] T in K, E and H in kJ/mol, and C_v in J/mol K. Standard deviations are calculated according to ref 7. [b] The long-range corrections are based on the assumption of an uniform benzene distribution. [c] Reference 14. [d] Reference 15.

The contribution to E and C_v from internal vibrations has been calculated from the normal frequencies[13] assuming a quantum mechanical harmonic oscillator. With these assumptions, we get

$$H_{(l,s)} = 3RT + E_v + E_{conf} \tag{7}$$

C_p and C_v are related by

$$C_p - C_v = (\alpha^2/\kappa)T\nu \tag{8}$$

where α is the isobaric expansivity, κ the isothermal compressibility, and ν the molar volume. C_p can thus be factorized according to

$$C_p = C_{v,t} + C_{v,r} + C_{v,v} + C_{v,conf} + (\alpha^2/\kappa)T\nu \tag{9}$$

and we get

$$C_{p(l)} = 3R + C_{v,v} + C_{v,conf} + (\alpha^2/\kappa)T\nu \tag{10}$$

Table IV gives the calculated configurational energy corrected for the finite system and the configurational contributions to C_v. A comparison between ΔH_{vap}^{calcd} according to eq 6 and ΔH_{vap}^{exptl} shows that the benzene potential may quantitatively give the enthalpy of evaporation over a wide temperature range. Another point worth mentioning is that the total contribution from the internal vibrations to the energy is well above RT except for the lowest temperature. By using 120 K as the reference state, we see that the enthalpy difference between the calculation and experiment deviates at most by 2 kJ/mol over a temperature range of about 230 K.

The isobaric expansivity and isothermal compressibility for benzene at room temperature is 1.24×10^{-3} K^{-1} and 9.09×10^{-10} Pa^{-1},[16] respectively, and thus $(\alpha^2/\kappa)T\nu \approx 45$ J/mol K at 308 K. Using the harmonic vibration assumption we get $C_{v,v} = 51.0$ J/mol K. Equation 10 together with $C_{v,conf}^{calcd}$ gives $C_p = 136$ J/mol K compared with $C_p^{exptl} = 138$ J/mol K.[15] However, since $C_{v,conf}^{calcd} \approx 0.1C_p$, this agreement shows mainly that other terms than $C_{v,conf}$ are consistent with experiment. In the case of water, both $C_{v,v}$ and $(\alpha^2/\kappa)T\nu$ are negligible, and $C_{v,conf} \approx 0.7C_v \approx 0.7C_p$, which makes it more fruitful to evaluate the heat capacity in a canonical ensemble with rigid molecules.

Figure 1 shows the distribution function of the pair energy. The pronounced structure at 120 K agrees with the radial distribution functions (see section IVC). At 258 K the rotational freedom about the C_6 axis (see section IVB) averages the distribution of the pair energy, and at 308 K the thermal motion (liquid state) reduceds further the probability of a large pair interaction.

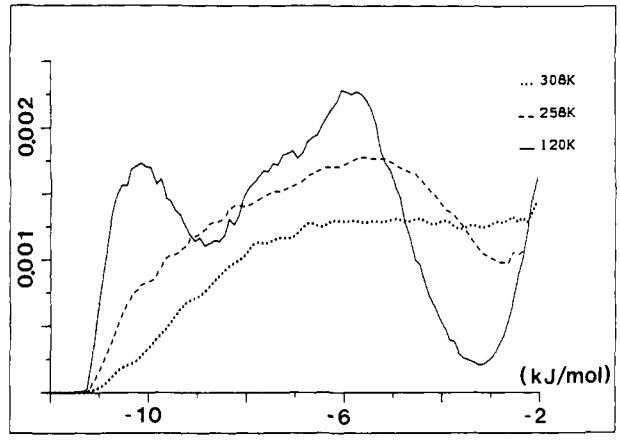

Figure 1. Distribution function of the molecular pair energy. The probability of pair energies above −2 kJ/mol increases rapidly and has a trivial maximum about 0 kJ/mol (not shown) due to numerous pairs with large separations.

B. Translation and Rotation Order. The structure changes in the system during the simulation were followed by the order parameters

$$O_t = (1/N)\langle \sum_{l=1}^{N} \cos(\boldsymbol{k}\cdot\boldsymbol{r}_l) \rangle \tag{11}$$

$$O_{r\alpha} = (1/2N)\langle \sum_{l=1}^{N} [3(\hat{U}_l^{\alpha}\cdot\hat{U}_{l0}^{\alpha})^2 - 1] \rangle \tag{12}$$

where O_t and $O_{r\alpha}$ refer to the translational and rotational order of the molecular axis α, respectively, and $\langle\cdots\rangle$ denotes an ensemble average. The vector $\boldsymbol{k}$ is $(2\pi/a, 2\pi/b, 2\pi/c)$, a, b, and c are the unit cell lengths, and $\boldsymbol{r}_l$ is the radius vector for the center of mass of molecule 1. The unit vector $\hat{U}_l^{\alpha}$ is attached to the benzene molecule, and $\hat{U}_{l0}^{\alpha}$ is its initial value. We will consider α equal to the C_6 axis and a C_2 axis through two hydrogens. The absolute value of O_t or $O_{r\alpha}$ is unity in a perfect face-centered-cubic lattice.

The order parameter O_t showed that no translational order remained after equilibration at 308 and 348 K. However, at the two lower temperatures we obtained $|O_t| > 0.8$ during the whole run. The rotational order is lost at the two higher temperatures, but also the order of the C_2 axes at 258 K is gradually lost, while O_{r,C_6} remains at 0.8. At 120 K both O_{r,C_2} and O_{r,C_6} remain close to unity, indicating a high rotational order.

The loss of the translational order between 258 and 308 K indicates a phase transition between liquid and solid benzene, compared to the experimental melting point of 278.7 K. Second-moment NMR data[17] indicate that the frequency of rotation around the C_6 axis is much higher than the frequency around a C_2 axis. Although a more careful comparison of experimental dynamic results with our static results is difficult, it is obvious that the potential describes a larger rotational freedom around the C_6 axis than that around a C_2 axis in solid benzene.

C. Radial Distribution Functions and Structure Factors. The relative positions of the atoms (C and H) and the center (M) of the molecules were examined by four radial distribution functions (g_{MM}, g_{CC}, g_{CH}, and g_{HH}). Neutron scattering and X-ray experiments may provide an intermolecular structure factor $h(k)$, which is a weighted sum of atom–atom structure factors h_{ij}, where

$$h_{ij}(k) = 4\pi\rho \int_0^{\infty} [g_{ij}(r) - 1] \frac{\sin kr}{kr} r^2 \, dr \tag{13}$$

In the case of neutron scattering from deuteriobenzene, the weight factors are k independent and almost identical and we have

$$h(k)^N \approx 0.25h_{CC}(k) + 0.50h_{CD}(k) + 0.25h_{DD}(k) \tag{14}$$

(13) Pitzer, K. S.; Scott, D. W. *J. Am. Chem. Soc.* **1943**, *65*, 803.
(14) Jordan, T. E., Ed. "Vapor Pressure of Organic Compounds"; Interscience: New York, 1954.
(15) "Selected Values of Properties of Hydrocarbons and Related Compounds"; Texas A&M University: College Station, Texas, 1979.
(16) Atkins, P. W. Ed. "Physical Chemistry"; Oxford University Press: London, 1982.
(17) Andrew, E. R.; Eades, R. G. *Proc. R. Soc. London, Ser. A* **1953**, *218*, 537.

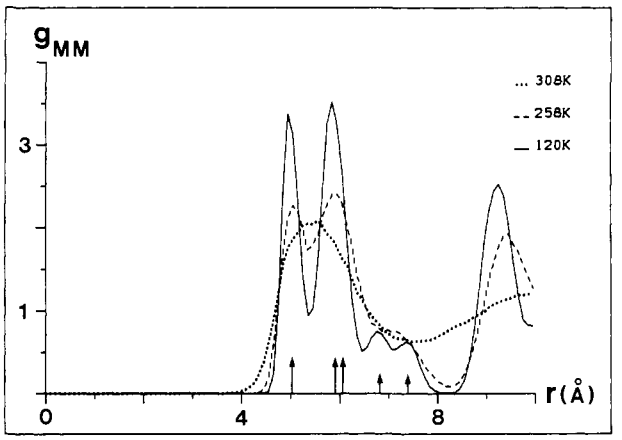

Figure 2. Center–center radial distribution function g_{MM}. The arrows show the positions in solid[19] rescaled from 138 to 120 K.

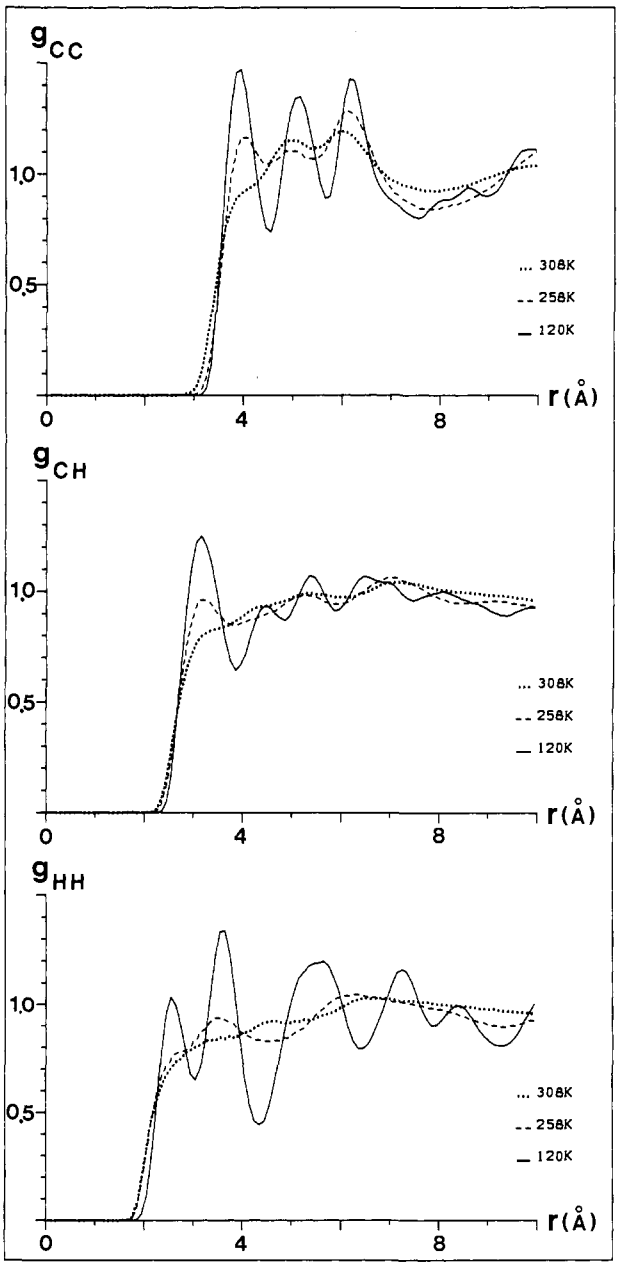

Figure 3. Atom–atom radial distribution functions g_{CC}, g_{CH}, and g_{HH}.

and a corresponding linear relationship for $g(r)^N$. Narten[18] has proposed an approximative interpretation of X-ray diffraction data,

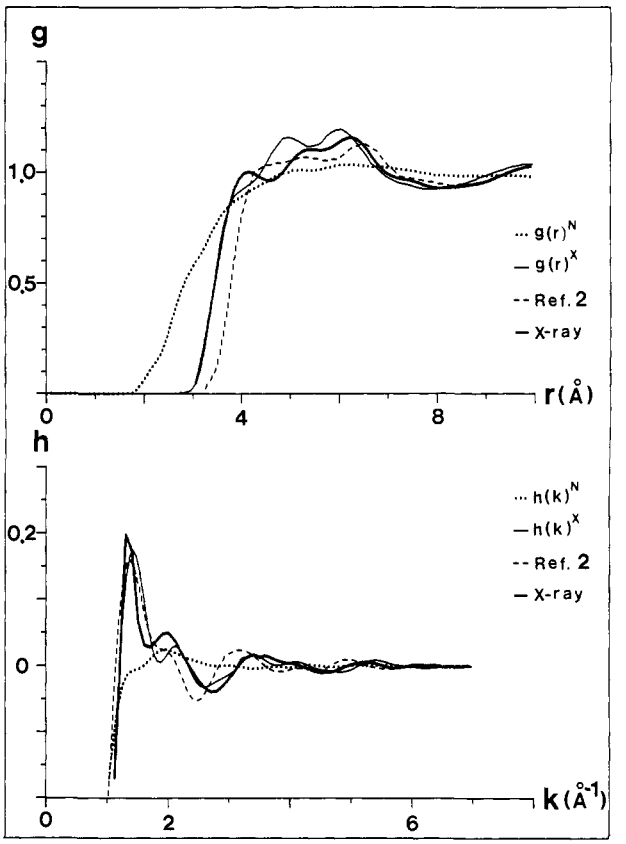

Figure 4. Experimental X-ray results[18] are compared with the calculated radial distribution function $g(r)^X$ and structure factor $h(k)^X$ obtained by eq 15 and with similar calculated results from ref 2. $g(r)^N$ and $h(k)^N$ show the calculated results expected from neutron scattering according to eq 14.

where the scattering density is decomposed into contributions from $(CH)_n$ groups rather than from C and H atoms. This treatment gives

$$h(k)^X \approx h_{CC}(k) \tag{15}$$

Figure 2 compares g_{MM} at three temperatures. The arrows show the corresponding center-to-center distances in the solid, experimentally obtained at 138 K[19] and rescaled to 120 K. The radial distribution functions and the atom–atom structure factors at 308 and 348 K are quite similar, and only those at 308 K will be reported here. The first maximum of g_{MM} at 120 K arises from the four symmetry-equivalent nearest neighbors, and the second maximum at about 5.9 Å corresponds to the four second and four third nearest neighbors. The following two peaks arise from pairs of equivalent molecules in different unit cells. A further analysis shows that the molecular separation of 4.5 Å at 120 K corresponds to a pair energy of about −10 kJ/mol (see Figure 1) and the following broad peak between −9 and −3 kJ/mol from distances up to 8.2 Å. At 308 K g_{MM} has a typical liquid behavior with a broad first maximum at 5.4 Å and its first minimum at 7.5 Å. This first peak corresponds to 11.9 molecules. In earlier simulations of liquid benzene with LJ site–site potentials,[1-3] g_{MM} displays a shoulder at 4.0 Å representing a stacked configuration. This stacked configuration does not appear here due to the repulsive quadrupole–quadrupole interaction in our potential. Figure 3 shows that g_{CC}, g_{CH}, and g_{HH} are strongly oscillating at 120 K, but at 258 K they resemble more the radial distributions in liquid at 308 K, due to the rotational freedom around the C_6 axis at 258 K which averages the otherwise oscillated structure. For the liquid

(18) Narten, A. H. *J. Chem. Phys.* **1968**, *48*, 1630; **1977**, *67*, 2102.
(19) Bacon, G. E.; Curry, N. A.; Wilson, S. A. *Proc. R. Soc. London, Ser A* **1964**, *279*, 98.

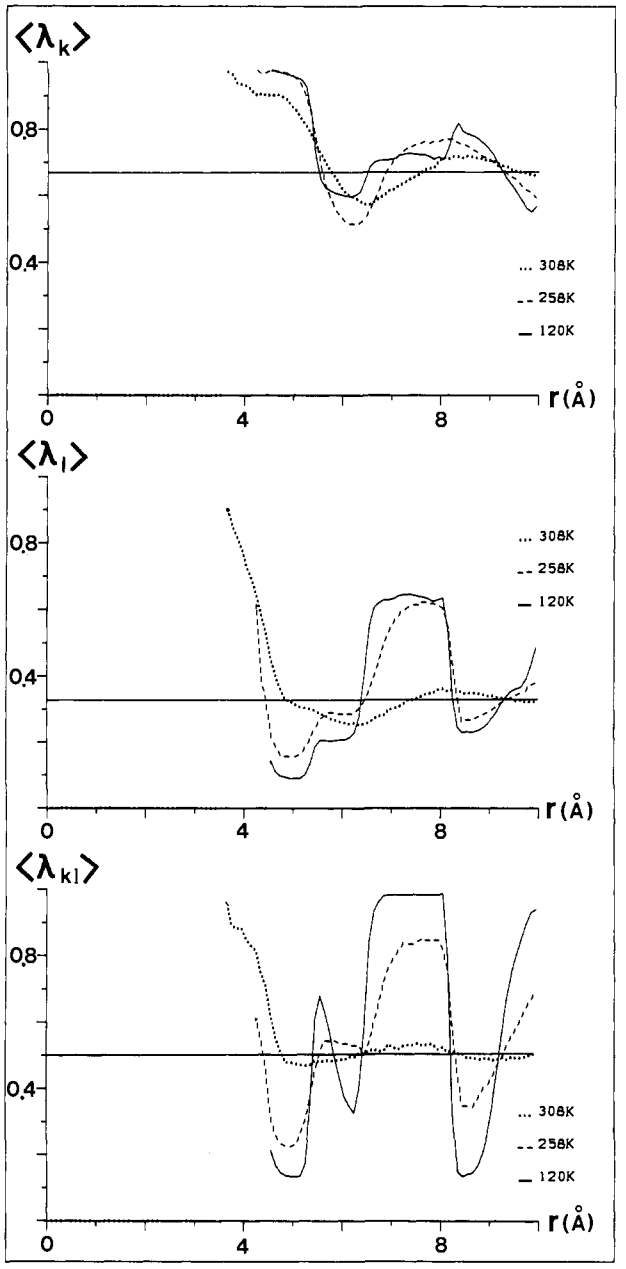

Figure 5. Functions $\langle\lambda_k\rangle$, $\langle\lambda_l\rangle$, and $\langle\lambda_{kl}\rangle$ show the average of the angular functions λ_k, λ_l, and λ_{kl} given by eq 16 as a function of the intermolecular center–center distance, r. The frequency of a distance between r and $r + dr$ is given by $4\pi r^2 g_{MM}(r)\,dr$.

state the atom–atom distribution functions show only a minor structure.

Figure 4 displays results from X-ray experiments by Narten[18] at 298 K with simulation results by Steinhauser[2] at 288 K and our $g(r)^X$ at 308 K. At larger distances, $r > 6.5$ Å, all three radial distribution functions agree quantitatively with each other. However, at shorter distances, 3–4 Å, the quantum mechanical potential is in perfect agreement with experiment while the LJ potential predicts a rise of $g(r)$ at about 0.4-Å larger separation. At intermediate separation, the two simulated curves only qualitatively reproduce the experimental results. Figure 4 shows also a very satisfactory agreement between the corresponding experimental structure factor and our simulated one given by eq 15.

The structure factor $h(k)^N$ given by eq 14 and $g(r)^N$ were calculated and are also shown in Figure 4. Both of them are poor on characteristic details due to large cancellations among g_{CC}, g_{CH}, and g_{HH}.

D. Orientation Structure. In order to facilitate comparison with earlier work,[1,3] we have followed Evans and Watts and defined three structure parameters by

$$\lambda_k = |\hat{U}_k^{C_6} \cdot \hat{r}_{kl}| \qquad (16)$$

$$\lambda_l = |\hat{U}_l^{C_6} \cdot \hat{r}_{kl}|$$

$$\lambda_{kl} = |\hat{U}_k^{C_6} \cdot \hat{U}_l^{C_6}|$$

where $\hat{r}_{kl}$ is the unit vector between the centers of mass of molecules k and l. The orientational averages at the distance r are denoted $\langle\lambda_k(r)\rangle$, $\langle\lambda_l(r)\rangle$, and $\langle\lambda_{kl}(r)\rangle$. The molecules are labeled in such a way that $0 \le \lambda_l \le \lambda_k \le 1$ gives the uncorrelated values of $^2/_3$, $^1/_3$, and $^1/_2$, respectively.

The structure parameters are displayed in Figure 5. The behavior at 120 K agrees very well with experimental lattice data at 138 K[19] and with the interpretation of g_{MM}. Figure 2 shows that nearest neighbors are separated by about 5 Å, and $\langle\lambda_k\rangle \approx 1$ and $\langle\lambda_l\rangle \approx \langle\lambda_{kl}\rangle \approx 0.1$ given by Figure 5 confirm the experimental finding[19] of perpendicular orientation. At 5.8 Å the experimental orientation is near parallel, and at 6.0 Å it is perpendicular, and Figure 5 shows this behavior, although temperature broadened. Finally, the calculated parallel orientation $\langle\lambda_{kl}\rangle \approx 1$ at separations between 6.8 and 8.0 Å is consistent with the fact that the pair of molecules is localized at the same symmetry point in adjacent unit cells.

At higher temperature and at short distances a more parallel orientation appears, which is almost perfect at 308 K at a separation of 3.6 Å. This is obvious, since the repulsive barrier for the perpendicular orientation starts at 4.5 Å[6] and a shorter separation favors a more stacked configuration. However, the *probability* for a stacked configuration is very small, according to Figure 2. At the more probable distances, 4.8 to 6.5 Å $\langle\lambda_{kl}\rangle$ is slightly lower than 0.50 indicating a small preference for perpendicular orientation, and at 6.5 to 8.5 Å we have the opposite case, which may be viewed as a reminiscence of the solid state. The orientation correlation given in Figure 3c in ref 3 expresses a similar pattern for the LJ + quadrupole potential.

E. Static Lattice Energy and Structure. At atmospheric pressure the crystal structure of benzene is orthorhombic with four molecules per unit cell.[12] Extrapolated lattice data at 0 K are given in Table V together with corresponding data obtained by minimizing the total energy of the crystal for two benzene potentials. These calculated data are obtained under the constraint that the space group is orthorhombic by variation of the six lattice parameters.

The benzene potential used in this work gives a very good agreement with the extrapolated orientational data. The lengths of the unit cell axes are less well reproduced, and the unit cell volume is underestimated by about 10%. Table V shows that the static lattice energy obtained is about 20% too low. An orientational optimation at experimental density reduces the energy difference to 10%, still too attractive.

The LJ and LJ + quadrupole potential[3] (the latter is not shown in Table V) are better in reproducing the unit cell volume and lattice energy but are not satisfactory regarding the Euler angles.

Table V. Experimental and Calculated Lattice Parameters for the Orthorhombic Benzene Crystal at 0 K[a]

	exptl[b]	LJ[c]	this work
a, Å	7.3 ± 0.2	7.10	7.19
b, Å	9.2 ± 0.3	9.52	8.74
c, Å	6.6 ± 0.1	6.96	6.35
θ, rad	0.80	0.825	0.80
ϕ, rad	0.42	0.000	0.40
ψ, rad	1.51	1.571	1.53
cell volume, Å	443.3	470.4	399
E, kJ/mol	−52.3	−44.54	−62.5

[a] a, b, c are the orthogonal unit cell axes and θ, ϕ, ψ are the Euler angles specifying the molecular orientation.[5] [b] Extrapolated to 0 K, ref 5. [c] Reference 3.

V. Conclusions

We have demonstrated that the quantum chemical benzene potential by Karlström et al.[6] can be used to calculate static

quantities with a surprisingly good agreement with experiments. The potential is generally an improvement over the existing empirical ones.[1-3] By examining different potential expressions we have shown that both a quadrupole moment and an explicit treatment of hydrogens are important to obtain an acceptable functional agreement with quantum chemical data.

The reference interaction site model (RISM) has been used by Lowden and Chandler[20] and by Narten[18] in describing the structure of liquid benzene. Narten[18] made the conclusion that the best twelve-site RISM molecule gave a significantly better agreement with experimental X-ray results than that found for a six-site model. Since the gist of the RISM approach is the short-range repulsive interaction, this conclusion is an argument supporting the importance of an accurate description of the molecular extension. However, a twelve-site model has a drawback in simulations due to the large number of atom–atom interactions. In the case of benzene, this can partially be mastered by using a simplified potential at separations where the interaction in reality is isotropic. If the isotropic interaction is sufficiently small, a spherical cutoff[9] is an alternative way to reduce the number of interactions.

Solid benzene at low temperature may be characterized by both a high-translational and -orientational order, and molecules close to each other prefer a perpendicular orientation. At higher temperature the rotation about the C_6 axis tends to destroy the orientational order of the C_2 axes and averages out the previously pronounced atom–atom distribution function. In the liquid state there is only a small orientational correlation between two molecules except at very short distances where the anisotropic exchange repulsion favors the stacked configuration. This is, however, counteracted by the repulsive quadrupole–quadrupole interaction, and the stacked configuration at short separations is infrequent.

The small existing disagreement between experimental data and calculated results indicates that the quantum chemical calculated potential gives a slightly too small molecule and as a result a too attractive pair energy.

Other investigations[21] have shown that the quantum mechanical approach given by Karlström et al.[6] leads to molecular potentials where the exchange repulsion is slightly underestimated. This underestimate of the exchange repulsion is due to the lack of diffuse basis functions which gives a deeper interaction minimum at a shorter intermolecular distance.

These simulations are based on a pair potential. In order to improve a theoretical description of liquid and solid benzene, the many-body effect of the interaction has to be considered. Also, the classical treatment and the neglect of internal vibrations restrict the possible accuracy of the model.

Acknowledgment. Stimulating discussions with and valuable criticism of the manuscript by B. Jönsson, G. Karlström, B. Lindman, and H. Wennerström are gratefully acknowledged. Thanks are due to S. Linse for helpful program development. A grant from Stiftelsen Bengt Lundqvists Minne is also gratefully acknowledged.

Registry No. Benzene, 71-43-2.

(20) Lowden, L. J.; Chandler, D. *J. Chem. Phys.* **1974**, *61*, 5228.

(21) Karlström, G., private communication.

Electronic Structure and Optical Spectrum of *cis*-Diammineplatinum α-Pyridone Blue: Metal–Metal Bonding and Charge Transfer in a Four-Atom Pt(2.25) Chain

Alvin P. Ginsberg,*[1a] Thomas V. O'Halloran,[1b,c,d] Phillip E. Fanwick,*[1e] L. Steven Hollis,[1c] and Stephen J. Lippard*[1c,d]

Contribution from AT&T Bell Laboratories, Murray Hill, New Jersey 07974, the Department of Chemistry, University of Kentucky, Lexington, Kentucky 40506, the Department of Chemistry, Columbia University, New York, New York 10027, and the Department of Chemistry, Massachusetts Institute of Technology, Cambridge, Massachusetts 02139.
Received January 10, 1984

Abstract: Polarized single-crystal optical spectroscopy, together with a scattered wave Xα analysis, provides an understanding of the intriguing blue color and the metal–metal interactions in the Pt(2.25) chain complex *cis*-diammineplatinum α-pyridone blue (PPB), *cis*-$[Pt(NH_3)_2(C_5H_4NO)]_4(NO_3)_5 \cdot H_2O$. Pt–Pt bonding is found to be mainly due to σ overlap between Pt d_{z^2}, s hybrid orbitals. The net σ-bonding interaction between the end pairs of Pt atoms in the chain is stronger than between the middle pair. The PPB HOMO and LUMO are Pt–Pt σ* in character and are delocalized over all four Pt atoms. Immediately below the HOMO are two orbitals with Pt–pyridone oxygen π* character. These orbital characteristics are used to rationalize the redox chemistry of PPB. Of the unpaired spin density 94% is contained within the Pt spheres, with 43% in the two end spheres and 51% in the two inner spheres. PPB is therefore a Robin–Day class III-A compound. The observed [and calculated] optical transition energies (eV), intensities, and polarizations are as follows: ~1.55 vw, ? [1.63 w, *x*]; 1.82 s, *z* [1.50 s, *z*; 1.53 s, *z*; 2.14 s, *z*]; 2.25 vw, *x* [2.15 vw, *x*; 2.16 vw, *x*; 2.39 vw, *x*]; 2.58 m, *z* [2.80 s, *z*]; 2.69 wm, *x* [2.39 m, *x*]; 3.10 w, *x* [2.84 w, *x*; 3.10 w, *x*]. The blue color of PPB is due to the intense *z*-polarized transitions at 1.82 (680 nm) and 2.58 eV (480 nm). These may be described, respectively, as inner Pt–Pt bonding → inner Pt–Pt σ* and outer Pt–Pt π → outer Pt–Pt σ*. Both inner Pt → outer Pt and outer Pt → inner Pt charge transfer make important contributions to the intensity of the 680-nm band, while outer Pt → inner Pt charge transfer is the main contributor to the intensity of the 480-nm band.

Blue platinum complexes derived from the antitumor drug *cis*-diamminedichloroplatinum(II)[2] are of considerable current interest,[3] although they have been known for over a decade.[4] We previously reported the synthesis, X-ray crystal structure deter-

0002-7863/84/1506-5430$01.50/0